Chapter 2

Propagation Fundamentals & Literature Search

The performance of wireless communication systems depends on the radio wave transmission path between the transmitter and the receiver. Unlike wired channels that are stationary and predictable, radio channels are extremely random. In addition, electromagnetic wave propagation characteristics vary significantly over different frequency bands. Therefore it is vital to thoroughly understand the propagation characteristics and develop a channel model for the proposed wireless communication system before site-specific planning and deployment can be initiated. This chapter introduces radio propagation mechanisms and principles, primarily for LMDS applications. Impairments to the radio propagation, path loss model and small-scale fading effects are discussed. Issues pertaining to propagation of millimeter waves are also presented. Finally, the chapter elaborates on the effects of rain on radio wave propagation. The concepts and models presented are essential for understanding propagation measurements and results in Chapters 3 through 5 of this dissertation.

The chapter also presents an extensive literature survey on outdoor radio wave propagation measurements performed at 38 GHz and 60 GHz. Also, methodology and pertinent details of the proposed measurement campaigns are also included at the end of the chapter.

2.1 Introduction to Radio Wave Propagation

The mechanisms behind electromagnetic wave propagation are diverse, but can generally be attributed to reflection, diffraction and scattering [Rap99]. *Reflection* occurs when a propagating electromagnetic wave impinges upon an object that is large compared to the wavelength of the propagating wave. *Diffraction* occurs when the radio path between the transmitter and receiver is obstructed by a surface with irregular edges. This gives rise to bending of waves around the obstacle, even when a line-of-sight path does not exist between transmitter and receiver. *Scattering*, the third basic propagation mechanism, occurs when objects with dimensions smaller than the wavelength of the propagating electromagnetic wave obstruct the radio channel. In particular, foliage, rain, lamp posts, etc, induce scattering in a wireless communication system. Figure 2.1 shows the overall radio spectrum, general distribution of frequencies and corresponding wavelength values. LMDS frequencies belong to SHF and EHF frequency bands.

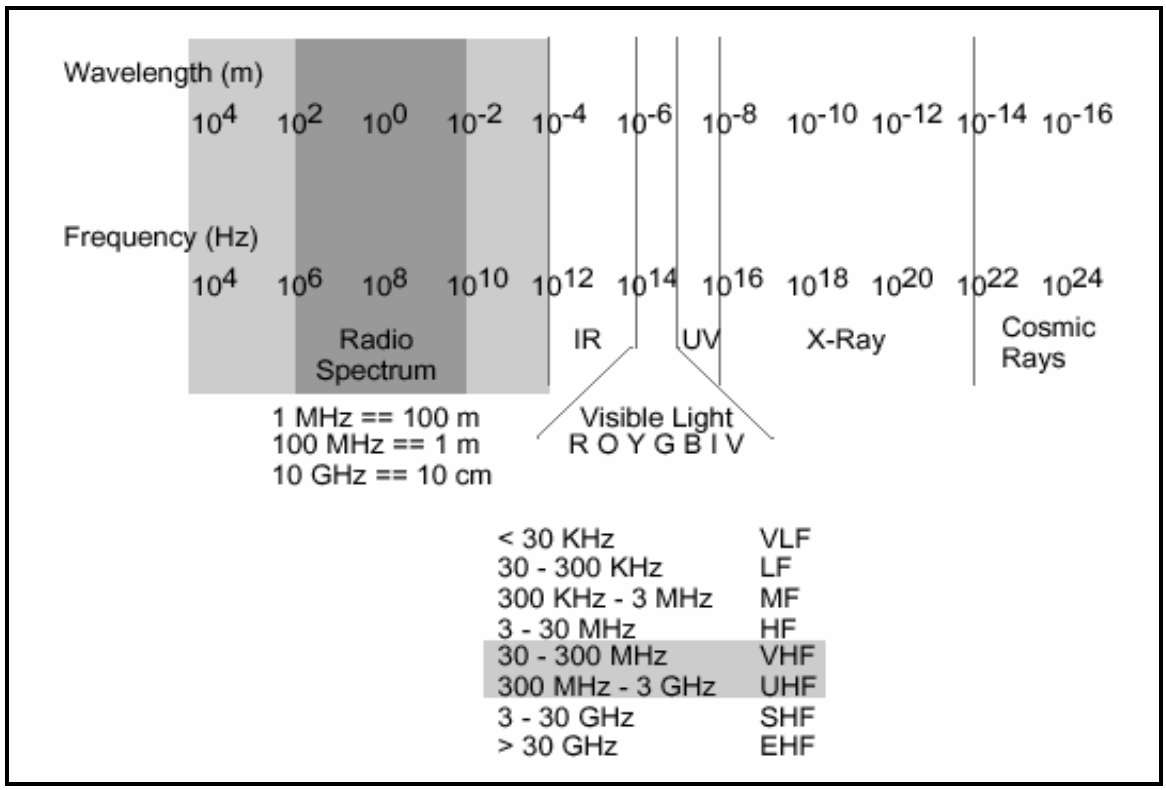

Figure 2.1 The frequencies in the Radio spectrum are classified into multiple groups. LMDS frequencies are a part of the SHF and EHF frequency bands. [Kat95]

2.1.1 Propagation Models

Propagation models that predict the mean signal strength for an arbitrary transmitter-receiver separation distance facilitate estimation of radio coverage area and are referred to as large-scale propagation models. On the other hand, propagation models that characterize the rapid fluctuations of the received signal strengths over very short distances or short time durations are called small-scale fading models.

2.1.1.1 Path Loss Models

The Path Loss, channel induced attenuation, may be defined as the difference (in dB) between the effective transmitted power and the received power; and may or may not include the effect of the antenna gains [Rap99]. This section presents Free Space Path Loss Model, Path Loss Exponent Model, and Partition based Path Loss Model.

Free Space Path Loss Model [Rap99]

The free space path loss model is used to predict received signal strength when the transmitter and receiver have a clear, unobstructed line-of-sight path between them. If d represents the transmitter-receiver separation distance and λ represents the wavelength of the propagating wave, then Equation 2.1 gives the Path Loss expression.

$$PL_{fs}(d)[dB] = 20\log_{10}(\frac{4pd}{l}) \qquad \textbf{Equation 2.1}$$

The Friis free space path loss model expressed by Equation 2.1 is valid only for distances that are in the far-field, or Fraunhofer region of the transmitter antenna. If D represents largest linear dimension of the antenna, d represents the transmitter-receiver (T-R) separation distance and λ represents the wavelength, then following relationships define the far-field region.

$$d >> D \qquad \textbf{Equation 2.2}$$

$$d >> l \qquad \textbf{Equation 2.3}$$

$$d >> \frac{2D^2}{l} \qquad \textbf{Equation 2.4}$$

Path Loss Exponent Model [Rap99]

Usually, a close-in distance, d_0, also referred to as the received power reference point, is introduced in Path Loss expressions. This reference distance is chosen such that it is smaller than any practical distance used in wireless communication systems and also such that it lies in the far-field region defined by Equations 2.2 through 2.4. If n represents the path loss exponent, which characterizes the relationship between increase in path loss values with increase in T-R separation distances, then path loss at a distance d (such that $d > d_0$) is given by Equation 2.5.

$$PL(d)[dB] = PL_{fs}(d_0)[dB] + 10n\log_{10}(\frac{d}{d_0}) \qquad \textbf{Equation 2.5}$$

The path loss exponent value depends on the obstructions in the radio channel. For free space line-of-sight propagation, the path loss exponent value is two [Dur98].

Partition Based Path Loss Model [Rap99]

This Path Loss Model estimates total path loss by adding the free space path loss and individual penetration losses caused by each obstruction. Let X_i represent penetration loss values for the i^{th} obstruction between the transmitter and receiver, then Equation 2.6 can be used to express the Partition based Path Loss Model.

$$PL(d)[dB] = PL(d_0)[dB] + 20\log_{10}(\frac{d}{d_0}) + \sum_{i=1}^{N} X_i[dB] \qquad \textbf{Equation 2.6}$$

2.1.1.2 Small-Scale Fading Model

Small-scale fading characterizes rapid fluctuations in the amplitude of a radio signal in a local area over short time intervals. The presence of reflecting objects or scatterers in the propagation channel results in multiple versions of the transmitted signal that arrive at the receiving antenna, displaced with respect to one another in time and spatial orientation [Rap99]. These multipath components can be completely characterized by their amplitude, phase, time-of-arrival, and angle-of-arrival information and superimposition of these multipath components results in small-scale fading and signal distortion. In addition to multipath propagation, small-scale fading is also affected by Doppler shifts on multipath components and the transmission bandwidth of the radio

signals. In a fixed broadband wireless communication system, moving objects in the radio propagation channel induce a time varying Doppler shift on multipath components. These multipath components contribute to Doppler spreading of the received signal, thus increasing the signal bandwidth [Rap99]. However, in most cases, the Doppler is small enough to be neglected.

2.1.2 Terrestrial Millimeter wave Propagation

Terrestrial Millimeter wave (mm-wave) outdoor wireless communication systems are primarily deployed in clear line-of-sight environments to avoid high penetration losses due to buildings and foliage. For these communication systems, in order to facilitate planning, installation and post deployment high-quality fiber-like system performance, it is vital to quantitatively and qualitatively characterize the terrestrial mm-wave propagation channels. Unfortunately, quantitative analysis of wideband mm-wave propagation channels is difficult to find in literature, particularly at 38 GHz and 60 GHz. This section enumerates primary issues pertaining to mm-wave propagation in outdoor radio channels and elaborates on diffraction effects. Absorption due to gases and scattering due to precipitation are included in the generalized path loss model. The next section of this dissertation presents the literature survey on outdoor propagation measurements performed in the 38 GHz and 60 GHz bands of frequencies.

The chief propagation effects that need to be considered in the design of fixed broadband microwave/mm-wave radio link are summarized as follows [ITU]:

- Line-of-Sight (LOS) and Fresnel Zone clearances
- Diffraction due to uneven terrain
- Frequency selective fading due to multipath
- Attenuation and scattering due to vegetation
- Attenuation due to atmospheric gases
- Attenuation and depolarization due to precipitation

These propagation effects can seriously degrade the system performance as a result of reduced system coverage and signal distortion due to frequency selective fading.

Transmission Losses

The Friis free-space propagation equation is commonly used to determine the attenuation of a signal due to the spreading of the electromagnetic wave. For frequencies between 500 MHz and 10 GHz, this model provides a good estimate of propagation loss. However, for frequencies above 10 GHz, losses due to molecular resonance and precipitation must be taken into consideration. The total transmission loss for a millimeter link is given by Freeman [Fre91] as:

$$\text{Atten (dB)} = 92.45 + 20\log_{10}(f_{GHz}) + 20\log_{10}(D_{km}) + \text{TExcess (dB)} \qquad \textbf{Equation 2.7}$$

$$\text{TExcess (dB)} = a + b + c + d + e \qquad \textbf{Equation 2.8}$$

where,

a = excess attenuation (dB) due to water vapor

b = excess attenuation (dB) due to mist or fog

c = excess attenuation (dB) due to oxygen (O_2)

d = sum of absorption losses (dB) due to other gases

e = excess attenuation (dB) due to rainfall

There are many atmospheric gases and pollutants that have absorption lines in the millimeter bands (such as SO_2, NO_2, O_2, H_2O, and N_2O), however the absorption loss is primarily due to water vapor and oxygen [Ula81].

Diffraction

Diffraction allows radio signals to propagate around the curved surface of the earth, beyond the horizon, and to propagate behind obstructions. The phenomenon of Diffraction can be explained by Huygen's principle, which states that all points on a wavefront can be regarded as point sources and give rise to secondary wavelets. Combination of all the wavelets produces a new wavefront in the direction of propagation.

Fresnel Zones represent successive regions where secondary waves have a path length from the transmitter to receiver which are $n\lambda/2$ greater than the total path length of a line-of-sight path. Fresnel zones are elliptical in shape with the transmitting and receiving antenna at their foci. The concentric circles, shown in Figure 2.2, represent boundaries of successive Fresnel zones. The successive Fresnel zones alternatively provide constructive and destructive interference to the

total received signal. The radius of the n^{th} Fresnel zone circle, denoted by r_n, can be expressed by Equation 2.9 [Rap99]. In Equation 2.9, λ represents the wavelength of the propagating wave and distance parameters d_1 and d_2 are explained in Figure 2.2. The expression is valid for $d_1, d_2 >> r_n$

$$r_n = \sqrt{\frac{n l d_1 d_2}{d_1 + d_2}} \qquad \textbf{Equation 2.9}$$

Diffraction losses occur when the secondary waves are blocked such that only a part of the energy is diffracted around the corner. The total received signal energy is given by the vector summation of energy contributions from all unobstructed Fresnel zones.

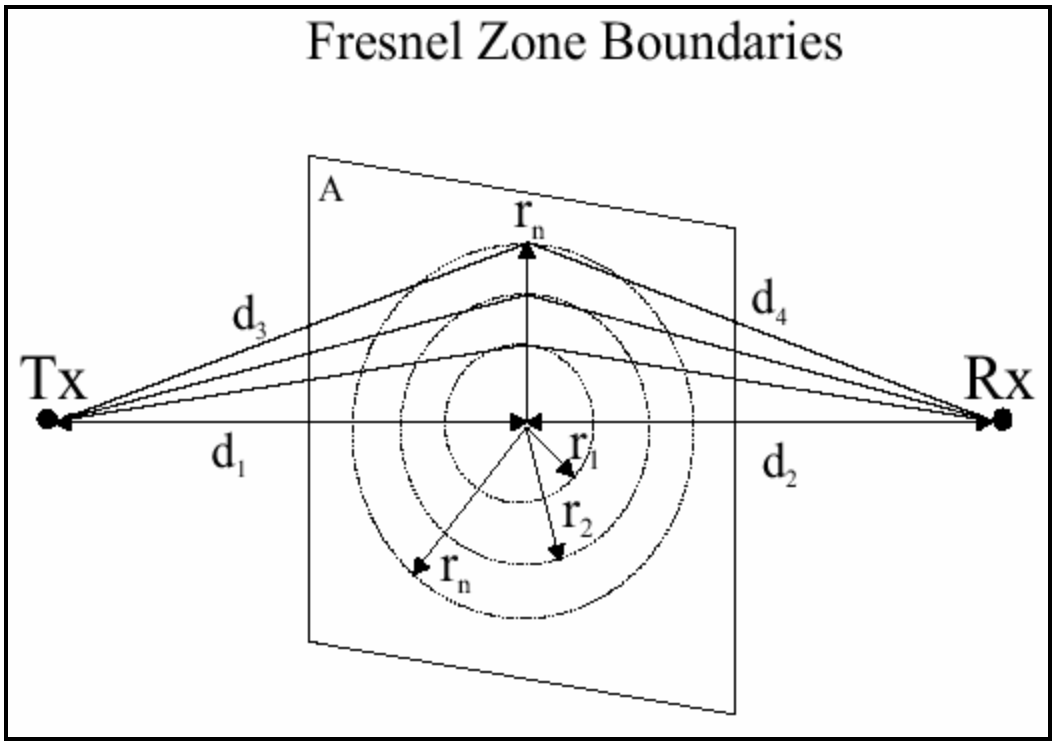

Figure 2.2 Concentric circles that define the boundaries of successive Fresnal zones [Hao00]

Knife-edge Diffraction model is one of the simplest diffraction models that is used to predict losses when diffraction shadowing is caused by a single object such as a hill or mountain. The model is shown in Figure 2.3 and Equations 2.10 and 2.12 express the Fresnel-Kirchoff Diffraction parameter and the Diffraction gain, respectively. It can be shown that the diffraction

losses increase with a decrease in the wavelength or increase in the frequency of the propagating electromagnetic wave.

$$\frac{E_d}{E_o} = F(v) = \frac{1+j}{2}\int_v^{\infty} \exp\left(\frac{(-jpt^2)}{2}\right)dt \qquad \textbf{Equation 2.10}$$

$$v = h\sqrt{\frac{2(d_1+d_2)}{l d_1 d_2}} \qquad \textbf{Equation 2.11}$$

$$G_d(dB) = 20\log|F(v)| \qquad \textbf{Equation 2.12}$$

In Equation 2.10, E_d is the electric field strength of the knife-edge diffracted wave while E_o is the free-space field strength in the absence of ground and knife-edge. Parameters used in Equation 2.11 are explained in Figure 2.3. G_d represents the diffraction gain in Equation 2.11.

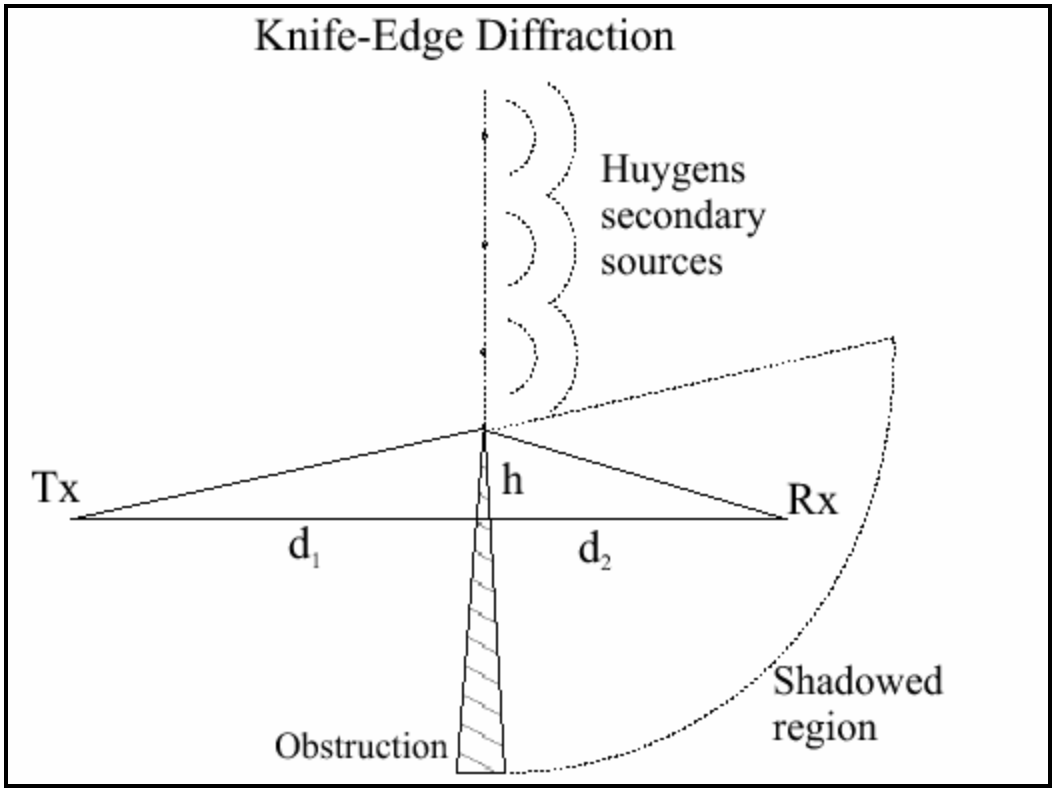

Figure 2.3 Knife-edge Diffraction Model [Hao00]

Scattering: Effects of Vegetation

When a radio wave impinges on a rough surface, the reflected energy is diffused in all directions due to scattering. At millimeter-wave frequencies, the dimensions of tree leaves, twigs, and tree branches are large as compared to the wavelength. The tree leaves and branches also usually contain water and hence result in absorption and scattering of electromagnetic waves as they propagate through vegetation. Foliage can not only introduce attenuation and broadening of the beam but also depolarization of the electromagnetic wave. The transmission losses through vegetation are affected by various parameters such as the dielectric constant, density, physical size and shape [Maj96].

International Telecommunications Union (ITU) recommends three different propagation models namely ITU-R, Fitted ITU-R (FITU-R) [Nua98], and the Nonzero Gradient (NZG) model [Sev95_1]. The ITU-R model was developed from propagation measurements performed at UHF. The transmitter and receivers are positioned such that most of the radio propagation path falls within the vegetation medium. The proposed model, presented in [Nua98], is stated to be applicable in the frequency range 200 MHz to 95 GHz. The fitted ITU-R (FITU-R) model attempts to optimize the ITU-R model while the NZG model is a more generalized model based on the maximum attenuation model but without a final fixed slope. For details please refer to [Sev95_1]. Another theory for millimeter wave propagation in woods and forests is formulated in [Sch88]. The transport theory, referred to as the theory of radiative energy transfer, is used to model radio wave propagation through woods and forests. For details, please refer to [Sch88] and [Whi96].

Scattering: Effects of Rain

Wireless communication systems operating at frequencies below 10 GHz are least affected by rain. However at millimeter frequencies, rain induced attenuation (due to absorption and scattering) is one of the principal factors that increases the overall path loss, limits the coverage area and consequently degrades the system performance. Extensive qualitative and quantitative analysis of effect of rain on the propagation of electromagnetic waves have been published in literature. Rigorous theoretical treatments of rain scattering can be found in ([Wol93], [Mor80],

[Mor79], [Ajo95]). Rain effects on satellite-to-ground propagation can be found in ([All89], [Pra86], [Stu95]).

The ITU recommends a calculation method for terrestrial systems, ITU-R P.530, and for satellite to earth links, ITU-R P.618 [ITU618]. The "Crane" models, after Robert K. Crane, are popular for satellite-earth links but also have terrestrial models. There are 3 versions of the Crane models. The Global Crane model was developed in 1980. In 1982 the 2-component Crane model was developed that used a path-integrated technique. A volume cell contribution and a debris contribution for a path were computed separately and added to provide a link calculation [Cra96]. As a refinement of the 2-component model, the revised two-component model was introduced in 1989 that includes spatial correlation and statistical variations of rain within a cell. All these models are included in [Cra96]. The theoretical prediction model proposed by Crane, based on the aR^b rain attenuation model, is summarized in Equations 2.13 through 2.18. In these Equations, A_R is the rain attenuation in dB, R is the point rain rate in mm/hr, and d is the distance in km. Constants 'a' and 'b' are rain attenuation coefficients that are functions of frequency and polarization and are tabulated in [Ols78].

$$A_R = aR^b\left[\frac{e^{ubd}-1}{ub}\right] \quad (for\ 0 \le d \le D_0) \qquad \textbf{Equation 2.13}$$

$$A_R = aR^b\left[\frac{e^{ubD_0}-1}{ub} - \frac{B^b e^{cbD_0}}{cb} + \frac{B^b e^{cbd}}{cb}\right] \ (for\ D_0 \le d \le 22.5\text{km}) \qquad \textbf{Equation 2.14}$$

where,

$$D_0 = 3.8 - 0.6\ln(R) \qquad \textbf{Equation 2.15}$$

$$B = 2.3R^{-0.17} \qquad \textbf{Equation 2.16}$$

$$u = \frac{\ln[Be^{cD_0}]}{D_0} \qquad \textbf{Equation 2.17}$$

$$c = 0.026 - 0.03\ln(R) \qquad \textbf{Equation 2.18}$$

For paths longer than 22.5 km, the attenuation A_R is calculated for a 22.5 km path, and the resulting rain attenuation is multiplied by a factor of (d/22.5).

Another empirical rain model based on nominal water droplet sizes and distribution by [Pra86] facilitates calculation of attenuation rate (dB/km) due to a specified rainfall rate. The model is referred to as the Simplified Attenuation Model (SAM/ CCIR). The attenuation rate can be approximately expressed by Equation 2.19, where R represents the rainfall rate in millimeters per hour and parameters 'a' and 'b' are respectively expressed using Equations 2.20 and 2.21.

$$k_{rain} = aR^b \qquad \textbf{Equation 2.19}$$

$a = 4.21 \times 10^{-5} f^{2.42}$ (for $2.9\text{GHz} \le f \le 54\text{GHz}$) **Equation 2.20.(a)**

$a = 4.09 \times 10^{-2} f^{0.669}$ (for $54\text{GHz} \le f \le 180\text{GHz}$) **Equation 2.20.(b)**

$b = 1.41 f^{-0.0779}$ (for $8.5\text{GHz} \le f \le 25\text{GHz}$) **Equation 2.21.(a)**

$b = 2.63 f^{-0.272}$ (for $25\text{GHz} \le f \le 164\text{GHz}$) **Equation 2.21.(b)**

It is important to note that in Equations 2.20 and 2.21, the frequency f is expressed in GHz.

2.2 Literature Survey

Numerous propagation measurement campaigns have been planned and executed to record and characterize the behavior of radio channels (at LMDS frequencies) in different environments and weather conditions. In [Vio88], Violette *et al.* presents line-of-sight (LOS) and NLOS micro/mm-wave propagation measurement performed over point-to-point links in Denver, CO. Continuous wave signal probes at 9.6, 28.8, and 57.6 GHz were used to measure signal loss over NLOS links. The paper quantitatively characterizes propagation losses through glass windows (simple and metalized), steel-reinforced concrete and brick walls over NLOS links. For LOS links with antenna heights of 2-3m, propagation measurements performed in streets indicate that reflected multipath components can result in fades in excess of 30dB. Linear antenna polarizations (VV and HH) were also compared to determine if mm-wave propagation in an urban environment shows any dependence on polarization. Influence of polarization on fading and delay spread in broadband radio channels at 30 GHz are also presented by Karthaus [Kar98]. The polarization diversity propagation measurements were performed at eleven locations for distances up to 3.8kms. It was concluded that for a given channel, different polarizations show very different performances concerning delay spread and multipath fading, but none of them works the best in all cases.

In [Pap96], a wideband propagation study performed at 28GHz frequency band, in a suburban neighborhood in Boulder, CO, is presented. Transmitter antenna heights were maintained at 16m and 40m while receiver antennas were positioned in residential buildings. The receiver antennas were raised 1 m above the house roof height and radio propagation measurements were recorded over radio link 2-7 km long. The study presents distribution of signal loss, delay spread and frequency selective fading over LOS links. The measurement results indicate that maximum delay spreads for the proposed antenna heights are limited to 10ns with a median value of less than 1ns. The results also indicate that attenuation due to vegetation is the primary propagation impairment for LMDS. Millimeter-wave propagation measurements (at 30.3 GHz) through a Pecan Orchard in Texas are presented in [Pap92]. Attenuation by rain and other propagation impairments at 28 GHz band of frequencies are analyzed in [Dal96]. In [Lin73], the statistical behavior of rain attenuation is analyzed and as many as 31 sets of experimental propagation data (terrestrial links and satellite-earth links) collected by different authors are summarized. Each of the terrestrial propagation measurements were performed over a period of at least 6 months for distances up to 80km at frequencies from 11 to 100 GHz. The results show that the distribution of rain attenuation is lognormal with a standard deviation ranging from 3.3 to 8.6 dB. Similar propagation campaigns in rain are analyzed in [Cra96].

Other propagation measurement campaigns, to facilitate planning, deployment and performance evaluation of LMDS systems at 28 GHz, are reported in ([Sei95], [Sei98]). In [Cor96], ray-tracing techniques are used to predict wideband channel impulse response for street level mm-wave propagation. Surface reflection is modeled using Snell's reflection coefficient and predicted results are shown to be in agreement with measured results.

2.2.1 Outdoor Propagation Measurements at 38 GHz

Outdoor propagation measurement results, characterizing an urban environment for wideband digital traffic, have been reported in [Hop91]. The measurements are primarily performed over LOS links and reflective properties of urban materials (metal, glass, wet flat roof surfaces etc) are quantified. The study employs a 90-degree transmitting horn antenna and a 20-degree

receiving horn antenna to record multipath structure and statistics. In [Wal93], results from a wideband channel sounding program, conducted at 39 GHz and 60 GHz, are summarized and a statistical model for wideband short-range mm-wave channels is presented.

Building scatter and vegetation attenuation measurement results at 38 GHz are elaborated in [Sev95_2]. The first section of the paper presents measured co-polar and cross-polar reflection profiles of a typical brick building. The results from CW measurements of specular and non-specular reflections of one face of a 2-storey building indicate that contribution from cross-polar reflections is generally lower than from co-polar non-specular reflection. Cross-polar effects are therefore less significant from the point of view of interference prediction. The attenuation measurements were performed through dense sycamore and lime trees with vegetation depths ranging from 0 to 46m. A standard gain pyramidal horn antenna was used as transmitter and receiver antenna heights were chosen as 3m, 5m and 7m from the ground level to facilitate propagation measurements at trunk level, foliage level and treetop level, respectively. Measured results indicate that signal attenuation due to vegetation varies with height and is minimal at the trunk level. Propagation results also indicate that signal attenuation increases sharply over shorter vegetation depths. However, as the vegetation depth increases, scattering from trees tends to contribute towards the received signal and hence the increase in signal attenuation is not as sharp. The paper also compares the measured attenuation statistics with the ITU recommended model and proposes an improved semi-empirical model based on the measured data at 38 GHz.

Other propagation measurement campaigns and results describing propagation effects due to building scatter and foliage at 38 GHz are reported in [Dil95] and [Sev97]. In [Maz95], Mazanek discusses depolarization caused by raindrops over a propagation link length of 52 m. The transmitting and receiving antennas are placed 32 m above the terrain throughout the propagation study. Theoretical attenuation for the vertical and horizontal polarization is shown as a function of the rain-rate at 37 GHz. Precipitation attenuation measurements at 40 and 60 GHz, and reflections measurements from snow-covered ground are also presented in [Tje97]. In ([Xu99], [Xu00], and [Hao00]), a measurement campaign that investigates weather effects on multipath dispersion and signal variation is presented. Wideband measurement campaigns are performed at

38 GHz on three point-to-point links, including a 605 m LOS link, a 265 m partially obstructed link and a 265 m link obstructed by vegetation. The results from propagation measurement campaigns, performed during clear sky, moderate to heavy rain and hail conditions, indicate that time dispersion characteristics of a radio channel may change during different weather events. In the study, fewer numbers of multipath components were detected during clear sky conditions than during moderate to heavy rain conditions. The results also show that received signal variation during rain follows a Rician distribution. In the paper, the rain attenuation statistics calculated from measured propagation data are compared with the Crane model. Upper and lower bounds for the Crane model are presented based on the measured rain attenuation data. The theoretical study, based on fundamental principles of wave propagation through random media of scatterers, also shows that non-uniform distribution of raindrop density along the propagation path can result in signal fluctuation.

2.2.2 Outdoor Propagation Measurements at 60 GHz

Electromagnetic wave propagation at 60 GHz band of frequencies experiences much higher path loss due to diffraction, scattering due to vegetation, scattering due to rain and oxygen absorption. Two propagation models for average path loss estimation and received power calculation at millimeter wave frequencies, specifically 60 GHz, are presented in [Cor94_1]. The first model adds a simple power to distance decay law to account for oxygen and rain absorption while the second model uses Geometrical Optics approach to model the electric field arriving at the receiver. The report also includes recorded impulse responses and results from propagation measurements performed in an urban street environment at 60 GHz. The results, from measurements over radio link lengths of 30 - 160 m, indicate that received power fluctuates by as much as 4 - 8 dB for LOS links due to multipath frequency selectivity and 6 - 8 dB for LOS links partially obstructed by trees. Other relevant publications by the author are ([Cor94_2], [Cor97]).

In [Lov94], the authors have presented consolidated wideband multipath measurement results from 7 different streets in downtown Oslo, each having different dimensions and traffic conditions. The paper describes the channel sounding equipment in brief and elaborates on

statistical distributions of instantaneous mean delay and delay spread. The results show that delay spread values are less than 20 ns for most of the measured urban street environments.

Fading characteristics along a canyon-like street at 60 GHz are studied in [Vas97]. In this measurement campaign, the transmitter, with a beam width of 25 degrees, was fixed in the middle of the street at a height of 3 m above the ground. An omni-directional slot antenna was used as the receiver. The results derived from the recorded measurements indicate that small-scale fading is well defined by Rician distribution in LOS street like environments.

Experimental results of LOS and NLOS radio propagation measurements, to characterize 62 GHz suburban micro-cell channels, are included in [Ham99]. During propagation measurements, the micro-cell base antenna was set at a height of 3.1 m while the receiver antenna height was maintained at 2.8 m above the ground. Propagation statistics were recorded at nine different locations to characterize the power and Angle of Arrival (AOA) statistics for multipath components. The paper concludes that a communication radio channel at 62 GHz band of frequencies can be adequately represented by a model that considers only LOS and second-order reflections from rough building surfaces and ground. The paper also presents and discusses in detail the mobile propagation measurement results.

In [Smu97], both narrowband and wideband, indoor as well as outdoor propagation measurement campaigns are described. The outdoor propagation measurements were recorded in airport field, urban street and city tunnel. Based on the results derived from recorded measurements, the paper concludes that city streets do not normally represent a severe multipath situation. Also, a road tunnel represents a very homogenous situation and has many similarities to the city street environment. The paper also concludes that simple ray-tracing tools and techniques may be used to satisfactorily ascertain radio channel characteristics. The simulation results for wideband characterization of propagation channel in urban streets using a ray-tracing tool, documented in [Cor96], relate well to the measured results. Other propagation measurement campaigns, characterizing path loss at 60 GHz band of frequencies, are presented in ([Haw95], and [Tha88]).

2.3 Proposed Measurement Campaigns

Wideband free-space (FS) propagation measurements over pico-cell radio links, documented in this dissertation, can be broadly classified as (a) The Path Loss Measurements, and (b) The Frequency Diversity Measurements. These measurement campaigns can be further classified on the basis of transmission frequencies, antenna polarizations, length of radio links and weather conditions. This section provides an introduction and some details relevant to proposed propagation measurement campaigns. The System Hardware and Calibration issues pertaining to the measurement campaigns are presented in Chapter 3 and an elaborate Measurement Plan is discussed in Chapter 4. The results, absolute path loss statistics in clear sky and rain, derived from these propagation measurements are analyzed in Chapter 5.

Path Loss Measurements

Site-specific Path Loss statistics plays an important role in planning and deployment of LMDS systems. Before any LMDS communication system can be designed and deployed, it is necessary to be able to predict worst-case path loss statistics for the proposed deployment location. Needless to mention, the best options is to measure the actual path loss values during different weather events over a fairly large period of time, for the specified location. However, in most cases, this is not feasible due to economic or time constraints. Numerous empirical based Path Loss models that take into account vegetation scattering, rain scattering and absorption due to atmospheric gases have been proposed in literature and may be effectively used to predict worst-case path loss statistics for a given location. Some of these models have also been described in Sections 2.1 and 2.2. The Path Loss measurements performed, as a part of the measurement campaigns in this research, were aimed at characterization of pico-cell scenarios. Data was recorded over LOS radio link lengths of 160m, 418m, and 531m. In each of the configurations, high placed and highly directional transmitting and receiving antennas were used to model a typical LMDS scenario. Path loss measurements were recorded at both 38 GHz and 60 GHz, with vertical antenna polarization, over three radio links on the Virginia Tech campus. At 38 GHz, horizontal antenna polarization propagation measurements were also recorded in

conjunction with vertical polarization measurements. Due to system hardware limitations, horizontal polarization measurements could not be recorded at 60 GHz. The path loss propagation measurements were recorded during clear sky conditions, for moderate to heavy rain conditions.

Frequency Diversity Measurements

In a multipath rich environment, frequency selective fading is often responsible for severe signal distortion and small-scale fading. The concept of frequency selective fading is briefly presented in Section 2.1.1 and discussed in detail in [Rap99]. In such an environment, electromagnetic wave propagation over a given link may exhibit different performance at different closely spaced carrier frequencies. In other words, frequency diversity can be exploited to achieve improved performance in a multipath rich environment that causes severe fades in the received signal. In an ideal scenario, the communication system will be able to scan the system performance at all the carrier frequencies available in the allocated band of frequencies and perform real-time switching/ selection of 'healthy' communication channels (carrier frequencies).

The frequency diversity propagation measurements in this research are aimed at characterizing the improvement in performance of LMDS communication systems operating in the 38 and 60 GHz bands of frequencies. These propagation measurements were recorded over 418m and 531m LOS radio links during clear sky conditions. The 12 different carrier frequencies studied, in the 38 and 60 GHz frequency bands each, are listed in Table 3.1. Results from the measurement campaigns are presented in Chapter 5.